

This is the post-print version of the following article:

de Barros, HR; García, I; Kuttner, C; Zeballos, N; Camargo, PHC; de Torresi, SIC; López-Gallego, F; Liz-Marzán, LM. [Mechanistic Insights into the Light-Driven Catalysis of an Immobilized Lipase on Plasmonic Nanomaterials](#), *ACS Catal.* 2021, 11, 1, 414–423

DOI: [10.1021/acscatal.0c04919](https://doi.org/10.1021/acscatal.0c04919)

This article may be used for non-commercial purposes in accordance with ACS Terms and Conditions for Self-Archiving.

1 Mechanistic insights on the light-driven catalysis of
2 an immobilized lipase on plasmonic nanomaterials

3 *Heloise R. de Barros,*^{a,b} Isabel García,^{b,c} Christian Kuttner,^b Nicoll Zeballos,^b Pedro H. C.*
4 *Camargo,^{a,d} Susana I. Cordoba de Torresi,^a Fernando López-Gallego,*^{b,e} and Luis M. Liz-*
5 *Marzán^{b,c,e}*

6 ^a Department of Fundamental Chemistry, Institute of Chemistry, University of São Paulo, Av.
7 Prof. Lineu Prestes, 748, Vila Universitária, 05508-000 São Paulo, SP, Brazil.

8 ^b CIC biomaGUNE, Basque Research and Technology Alliance (BRTA), Paseo de Miramón
9 182, 20014 Donostia – San Sebastián, Spain.

10 ^c Centro de Investigación Biomédica en Red, Bioingeniería, Biomateriales y Nanomedicina
11 (CIBER-BBN), Paseo de Miramón 182, 20014 Donostia – San Sebastián, Spain.

12 ^d Department of Chemistry, University of Helsinki, A.I. Virtasen aukio 1, Helsinki, Finland

13 ^e Ikerbasque, Basque Foundation for Science, 48013 Bilbao, Spain.

14 KEYWORDS biocatalysis, gold nanostructures, LSPR-enhanced mechanisms, nanotechnology,
15 plasmonic heating, triggered bioactivity.

16

17

18 ABSTRACT

19 The use of light as an external stimulus to control enzyme activity is an emerging strategy that
20 enables accurate, remote and noninvasive biotransformations. In this context, immobilization of
21 enzymes on plasmonic nanoparticles offers an opportunity to create light-responsive biocatalytic
22 materials. Nevertheless, a fundamental and mechanistic understanding on the effects of localized
23 surface plasmon resonance (LSPR) excitation over enzyme regulation remains elusive. We
24 investigate herein the plasmonic effects on biocatalysis using Au nanospheres (AuNSp) and
25 nanostars (AuNSt) as model plasmonic nanoparticles, lipase from *Candida antarctica* fraction B
26 (CALB) as a proof of concept enzyme, and 808 nm as NIR light excitation. Our data show that
27 LSPR excitation enables an enhancement of 58% in enzyme activity for CALB adsorbed on
28 AuNSt, compared with the dark conditions. This work shows how photothermal heating over the
29 LSPR excitation enhances CALB activity through favoring product release in the last step of the
30 enzyme mechanism. We propose that the results reported herein shed important mechanistic and
31 kinetic insights in the field of plasmonic biocatalysis and may inspire the rational development of
32 plasmonic nanomaterial-enzyme hybrids with tailored activities under external light irradiation.

33

34 INTRODUCTION

35 Plasmonic nanomaterials, such as gold nanoparticles (Au NPs), display remarkable optical
36 properties in the visible and near-infrared (NIR) spectral regions.¹⁻³ Such properties arise as a result
37 of the excitation of localized surface plasmon resonances (LSPRs). It has been established that
38 LSPR excitation in plasmonic NPs can accelerate a myriad of chemical transformations.⁴⁻⁷ This

39 catalytic effect can occur as a result of the generation of LSPR-excited charge carriers (hot
40 electrons and hot holes) and/or photothermal heating following plasmon decay.^{4,8,9} Surprisingly,
41 only a few studies have explored the use of LSPR excitation to tune biocatalytic reactions.¹⁰⁻¹⁵

42 The conjugation of enzymes to plasmonic NPs is attractive for applications in biomedicine,
43 such as photothermal therapy^{16,17} and bioimaging,¹⁸ as well as in chemical manufacturing.¹³ In fact,
44 the use of plasmonic effects at the interface between nanoparticles and enzymes is gaining
45 momentum as a tool to remotely control biocatalytic processes using light as an external
46 stimulus.^{12,13,19} This field, plasmonic biocatalysis, paves the way to tuning enzymes' properties in
47 a non-invasive manner, enabling spatio-temporal control over the biocatalytic processes.^{12,13}
48 Despite these fascinating opportunities, the mechanisms at the "nano-bio" interface underlying the
49 influence of plasmonic effects on enzyme functionality are poorly understood.^{10,12,20}

50 What is already known is that the enzyme/nanomaterial interface plays an important role
51 in the transport of substrates and products from the bulk to the enzyme active site, and *vice versa*,
52 thereby altering enzyme activity.²¹ For example, recent insightful mechanistic studies revealed that
53 the conjugation of hydrolases (*i.e.* phosphotriesterase) to quantum dots and Au NPs enhances the
54 enzymatic kinetic efficiency, as compared to their free counterparts.^{22,23} Furthermore, kinetic
55 studies under high viscosity conditions demonstrate that the increase in apparent catalytic rate (k_{cat})
56 relies on higher product release kinetic constants associated to the last step of the hydrolases
57 catalytic mechanism. Nevertheless, how those kinetic parameters may be altered by light at the
58 interface between enzyme and plasmonic nanomaterials is still an open question that remains
59 largely underexplored.

60 To bridge this gap, we report herein on a detailed and systematic study of the effects of
61 LSPR excitation over the activity and enhancement mechanisms in plasmonic biocatalysis.
62 Specifically, we selected the lipase from *Candida antarctica* fraction B (CALB) as a proof of
63 concept enzyme, whose catalytic mechanism is well understood, Au nanospheres (AuNSp) and
64 nanostars (AuNSt) as model plasmonic NPs, and a NIR laser as the light excitation source. Both
65 on- (AuNSs) and off- (AuNPs) resonance conditions relative to the NIR laser source were
66 investigated to demonstrate the LSPR-driven enhancement effects. Although CALB has been
67 previously conjugated to Au NPs,²⁴⁻²⁶ control over its catalytic activity through plasmonic effects
68 remains elusive. Our data suggest that the localized photothermal heating following LSPR
69 excitation plays an important role toward favoring the reaction step involving product desorption
70 from the biocatalytic active sites, ultimately leading to increased reaction rates.

71 RESULTS AND DISCUSSION

72 The first step toward this study comprised CALB adsorption onto Au NPs. It is well
73 established that enzymes can interact with Au NPs surfaces via the interaction of carboxyl and
74 amine groups present in the amino acid residues of the enzyme structure, following a kinetic
75 process that involves anchoring, crawling, and subsequent binding onto the NPs surface.^{24, 27, 28} It
76 has also been reported that electrostatic binding can take place between remaining carboxyl groups
77 on the Au NPs' surface (*e.g.* from citrate employed during synthesis) and amino groups (*e.g.* Lys
78 and Arg) from the enzyme structure.²⁹ Furthermore, enzymes containing thiolated amino acid
79 residues may interact with the Au NPs surface by chemisorption.^{30, 31} CALB presents ten thiolated
80 residues in its structure, of which four are methionine and six are cysteine residues, forming three
81 disulfide bonds³² and providing favorable conditions for anchoring enzymes onto the NPs
82 surface.²⁷

83 AuNSt were synthesized by a seed-mediated growth method,^{33, 34} using ascorbic acid as
84 reducing agent, silver nitrate to assist the growth of spiky nanostructures, and CALB as stabilizing
85 molecule. AuNSp were synthesized according to the Turkevich method³⁵ and subsequently coated
86 by CALB. Both AuNSt and AuNSp were washed by centrifugation and removal of the supernatant
87 to ensure that only CALB molecules adsorbed onto the NPs surface. AuNSt and AuNSp showed
88 great colloidal stability upon CALB adsorption. The corresponding nanobioconjugates are referred
89 to as AuNSt@CALB and AuNSp@CALB, respectively. Figure 1A-D shows representative TEM
90 images AuNSp@CALB (Figure 1A and B) and AuNSt@CALB (Figure 1C and D). Nanoparticle
91 size distribution histograms are presented in Figure S1. The images confirm the formation of Au
92 nanospheres and nanostars with spiky morphology and sharp tips branching out from a central
93 core. Both AuNSt@CALB and AuNSp@CALB displayed a relatively narrow size distribution,
94 with diameters corresponding to 12 ± 2 and 100 ± 20 nm, respectively. For AuNSt, the tip
95 dimensions were approximately 45 ± 5 nm in length and 5 ± 0.6 nm in width. Although not
96 conclusive, high-resolution TEM images (Figure 1B and D) evidenced the presence of an organic
97 layer on AuNSp and AuNSt surfaces, which may correspond to adsorbed CALB. The
98 morphologies of AuNSp and AuNSt were thus preserved upon CALB adsorption and no
99 aggregation was observed, even after laser irradiation (Figure S2). This indicates that CALB
100 served as a suitable stabilizing agent for both AuNSp and AuNSt. AuNSp@CALB and
101 AuNSt@CALB exhibited intense LSPR bands around 525 nm and 700 nm, respectively (Figure
102 1E). These LSPR band positions were exploited to study the effect of on and off resonance
103 conditions, relative to the NIR laser wavelength employed in CALB biocatalysis studies (808 nm,
104 indicated by the dashed line in Figure 1E).

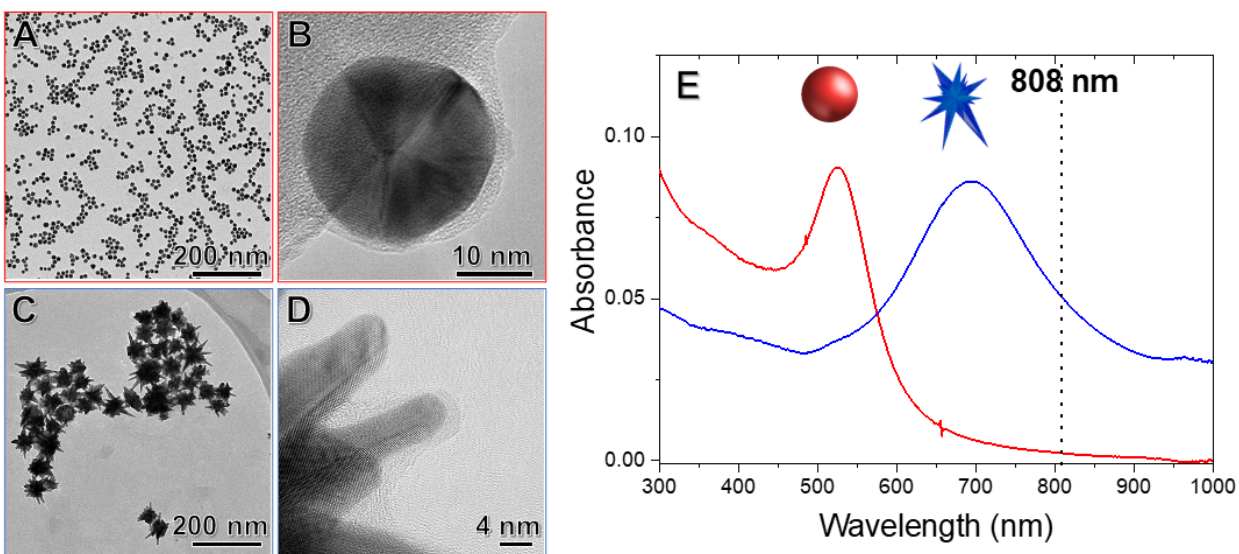


Figure 1. (A-D) TEM (A and C) and high resolution TEM (B and D) images of AuNSp@CALB (A and B) and AuNSt@CALB (C and D). (E) UV-Vis extinction spectra registered from aqueous suspensions containing of AuNSp@CALB (red trace) and AuNSt@CALB (blue trace). The 808 nm wavelength employed for biocatalysis studies is indicated by the black dashed line.

105

106 We then turned our attention to the study of CALB activity toward the hydrolysis of 4-
 107 nitrophenyl palmitate (*p*NPP) as a model reaction (see Scheme 1 in the Experimental section). We
 108 found that CALB activity (under light off conditions) decreased upon its adsorption on both AuNSt
 109 and AuNSp (Table 1). This behavior is a common trend typically observed for immobilized
 110 enzymes, being established that external mass transport restrictions limit their activity.³⁶ We
 111 determined the catalytic rate constant (k_{cat}), the binding Michaelis constant (K_M), and the catalytic
 112 efficiency (k_{cat}/K_M) of free CALB and the same apparent parameters for the adsorbed enzyme
 113 (Table 1 and Figure S3). Under light off conditions, the decrease in k_{cat} values for CALB adsorbed
 114 on the Au NPs can be related to a partial loss of enzyme activity. Nevertheless, the K_M values of
 115 adsorbed enzymes on the Au NPs were significantly smaller as compared to free CALB. This
 116 lower apparent K_M suggests an increase of substrate local concentration at the NP surface, which
 117 causes the higher activities observed at lower bulk substrate concentration. This effect was more

118 evident for AuNSt than for AuNSp. Similar results were obtained with a homologous lipase from
 119 *Candida rugosa* immobilized on AuNSp.²⁶ The k_{cat}/K_M value decreased upon CALB adsorption on
 120 the Au NPs, but that decay was 1.7 times lower for AuNSt@CALB than for AuNSp@CALB. The
 121 different kinetic behavior of CALB on the two different NP morphologies can be related to the
 122 enzyme density for nanoparticles with different curvature, where NPs with a smaller size (*i.e.*, with
 123 a higher curvature) display a higher enzyme activity.²³ In this context, the tips of AuNSt (*ca.* 5 nm
 124 in diameter) can provide a surface of much higher curvature, compared to AuNSp (diameter around
 125 20 nm), leading to a lower density of CALB at the NP surface that results in a higher enzyme
 126 activity.

127 **Table 1.** Kinetic parameters determined from Michaelis-Menten plots (Figure S3) for samples
 128 under light on and off (dark) conditions ^a.

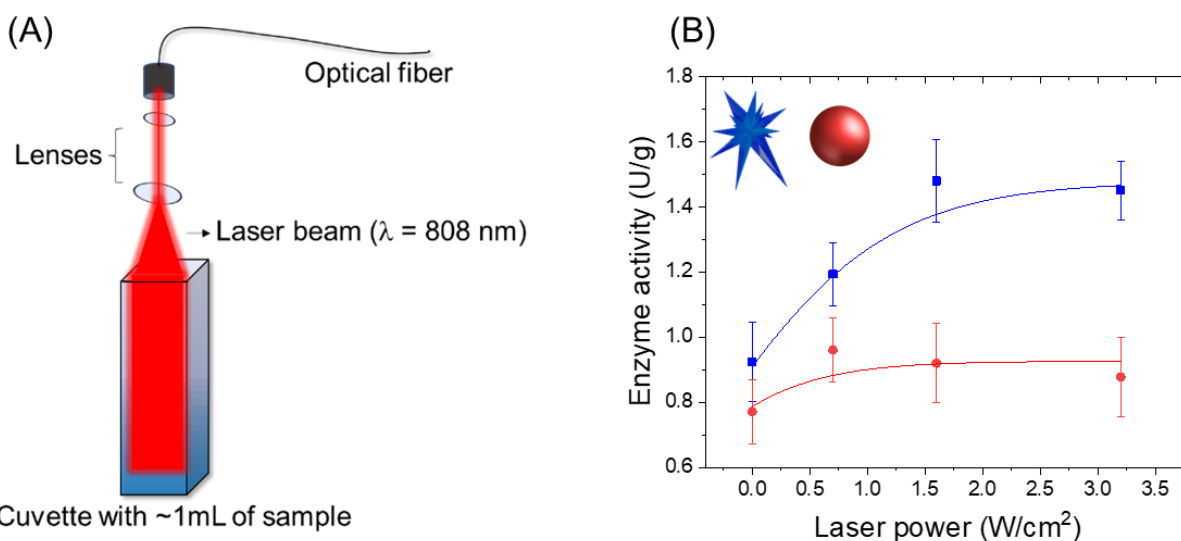
Sample	k_{cat} (min ⁻¹)		K_M (μM)		k_{cat}/K_M (μM ⁻¹ x min ⁻¹)	
	OFF	ON	OFF	ON	OFF	ON
AuNSt@CALB ^b	2461 ± 82	3947 ± 240	3.2 ± 0.4	5.1 ± 0.5	773 ± 180	765 ± 448
AuNSp@CALB ^c	2140 ± 126	2705 ± 372	4.8 ± 0.6	7.0 ± 2.0	443 ± 192	385 ± 186
Free CALB ^d	15855 ± 732	15966 ± 758	10.4 ± 4.3	9.7 ± 3.9	1520 ± 169	1640 ± 192

129 ^a Reaction conditions: PBS buffer at pH 7.4; at room temperature (approx. 20 °C); NIR laser irradiation at 3.2 W/cm².
 130 Enzyme concentration used: ^b 1.5 μmol L⁻¹, ^c 1.0 μmol L⁻¹, and ^d 1.1 μmol L⁻¹. The kinetic constants calculated for the
 131 immobilized enzymes are apparent constants, since they also account for mass transfer restrictions.

132

133 We further studied the effect of light irradiation on the hydrolytic activity of
 134 AuNSt@CALB and AuNSp@CALB under different irradiation conditions. The reactions were
 135 carried out in a quartz cuvette illuminated with a NIR laser at $\lambda = 808$ nm, measuring the release

136 of 4-nitrophenolate (*p*NP) *in situ*, using a UV-Vis spectrophotometer (Figure 2A). Unlike the
137 results under dark conditions, NIR irradiation enhanced the enzymatic activity of AuNSt@CALB
138 to a significantly higher extent than that for AuNSp@CALB irradiated under the different laser
139 powers (Figure 2B and Table 1). This result agrees with the better match between the incoming
140 light wavelength (808 nm) and the LSPR position in AuNSt (700 nm, Figure 1E), as compared to
141 AuNSp (525 nm, Figure 1E). In the case of AuNSt@CALB, the activity increases with laser power
142 until reaching a plateau at laser powers above 1.6 W/cm². No differences were observed for the
143 activity of free CALB under light on and off conditions (Figure S4). Therefore, NIR irradiation
144 only leads to a significant enhancement on the activity of CALB molecules at the surface of



145 AuNSt, which feature a LSPR position which better matches the light excitation wavelength.

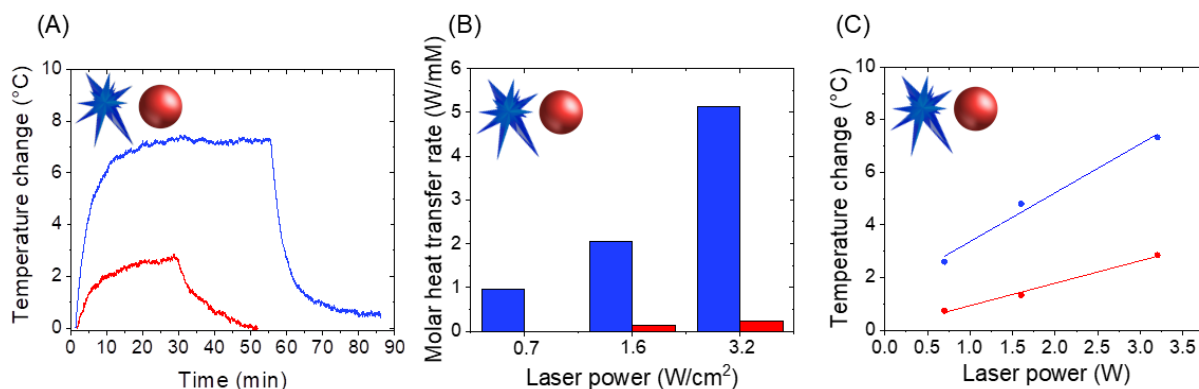
146
147 **Figure 2.** (A) Schematic illustration of the laser irradiation setup. (B) Effect of NIR laser power
148 ($\lambda = 808$ nm) on the enzymatic activity of AuNSt@CALB (blue squares) and AuNSp@CALB (red
149 circles).

150
151 To unravel the effect of LSPR excitation over enzymatic activity, we investigated the
152 heating capacity of AuNSt and AuNSp under the employed light irradiation conditions. The

153 samples were therefore illuminated with the NIR laser and the temperature changes in the colloidal
154 dispersion over time were monitored with a thermal camera. When the temperature reached
155 thermal equilibrium, the laser was turned off and the cooling down curve was recorded to quantify
156 heat dissipation to the solution. Figure 3A shows exemplary heating and cooling curves for both
157 AuNSt@CALB and AuNSp@CALB. The molar heat transfer rates for both AuNSt and AuNSp
158 were calculated by fitting these temperature time-courses to Equation 1,³⁷ as illustrated in Figure
159 3B.

$$160 \quad \frac{\Delta Q}{c_{Au}} = \frac{Q_{sample} - Q_{medium}}{\epsilon_{400}/2.4 \text{ mmol L}^{-1}} \quad (1)$$

161 Here, the generated heat output (ΔQ), obtained from the heat difference between the sample
162 (Q_{sample}) and the medium (Q_{medium}), is related in terms of the estimated gold concentration ($c_{Au} =$
163 $\epsilon_{400}/2.4 \text{ mmol L}^{-1}$)³⁸ in the sample. It was found that the molar heat transfer rate was much larger
164 for AuNSt@CALB than for AuNSp@CALB. In this case, LSPR excitation leads to photothermal
165 heating because of plasmon decay. Such a photothermal heating effect takes place close to the
166 NPs' surface and is further dissipated to the reaction mixture, leading to the detected temperature
167 increase. Our data indicate that AuNSt are more efficient nano-sources of heat⁸ than AuNSp under
168 the employed NIR irradiation conditions. In fact, Figure 3C shows that AuNSt@CALB under NIR
169 irradiation (3.2 W/cm^2) were capable to increase the bulk temperature of the reaction mixture up
170 to $7.3 \text{ }^\circ\text{C}$, versus the $2.7 \text{ }^\circ\text{C}$ observed for AuNSp@CALB under the same conditions. As expected
171 from the photothermal heating triggered by LSPR excitation, we observed an increase of the bulk
172 temperature by increasing the laser power.



173

174 **Figure 3.** Plasmonic heating effects of NIR laser ($\lambda = 808$ nm) on AuNSt@CALB (blue) and
 175 AuNSp@CALB (red). (A) Example of heating and cooling curves (laser power 3.2 W/cm²). (B)
 176 Molar heat transfer rate vs. laser power. (C) Temperature changes measured in colloidal
 177 dispersions of AuNSt@CALB (blue) and AuNSp@CALB (red).

178

179 In this context, it is expected that photothermal heating can lower the activation energy of
 180 the enzyme, according to the Arrhenius analysis²², thereby leading to higher enzyme activity. This
 181 effect was further confirmed by activity assays for both free CALB and adsorbed onto Au NPs,
 182 under different temperatures, as shown in Figure 4A. Typically, each class of enzyme exhibits an
 183 optimal temperature where the highest activity is observed.³⁹ Above this value, the activity
 184 gradually decreases due to protein denaturation. Free CALB showed an optimal temperature of 55
 185 °C (Figure 4A), in agreement with previously reported data.⁴⁰ At temperatures above 55 °C, free
 186 CALB undergoes thermal deactivation and its activity decreases considerably. Conversely, the
 187 enzymatic activity increased with temperature, even at values above 55 °C, for AuNSt@CALB
 188 and AuNSp@CALB. The preservation of enzyme activity at high temperatures indicates that the
 189 adsorption of CALB on Au NPs enhances the enzyme thermal stability. Circular dichroism (CD)
 190 spectroscopy studies (Figure 4B and Figure S5) demonstrate the higher conformational stability of
 191 enzymes adsorbed on both AuNSt and AuNSp, which explains their higher enzyme activities at
 192 temperatures above 55 °C. The observed decrease in mean residue ellipticity (MRE) at 222 nm

193 corresponds to major conformational changes in the α -helix secondary structure of CALB (Figure
194 4B). The adsorption of CALB on AuNSt precludes the structural distortions induced by the higher
195 temperatures, as no significant ellipticity changes were observed up to 48 °C. However, the
196 conformation of free CALB was gradually distorted at temperatures higher than 25 °C.

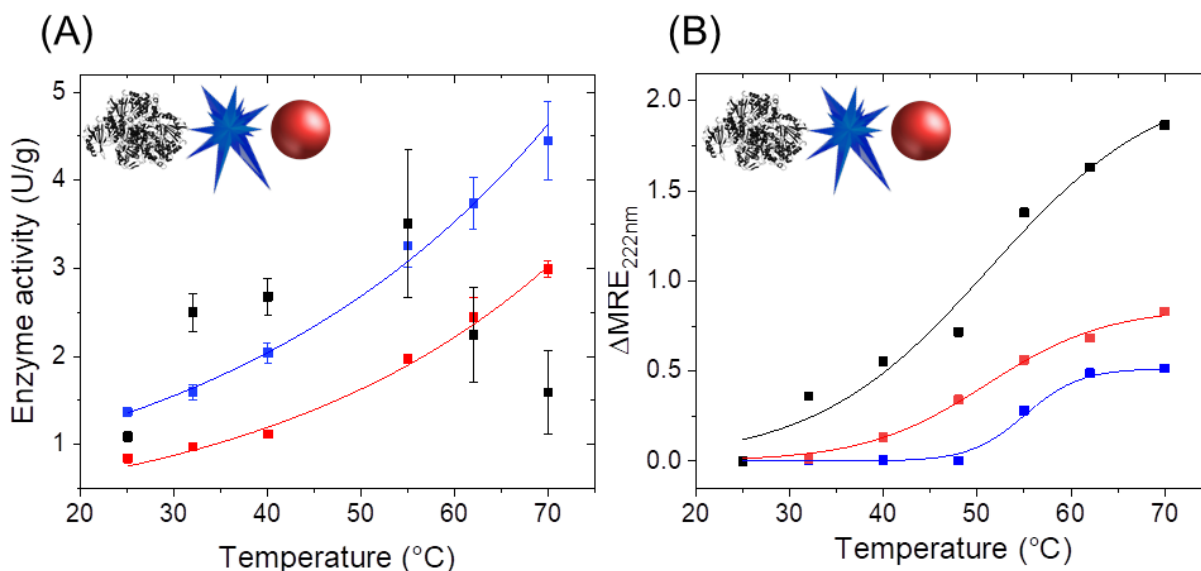


Figure 4. Temperature effects at dark conditions on enzymatic activity (A) and enzyme secondary structure (B), for AuNSt@CALB (blue), AuNSp@CALB (red), and free CALB (black). (A) Enzymatic activity as a function of temperature, fitted to the Arrhenius model. (B) Thermal denaturation of the enzyme conformation monitored by the variation of MRE ($\Delta MRE = MRE_{25^\circ C} - MRE_T$) at 222 nm, measured by CD spectroscopy. **CD data were obtained by an average of 10 accumulation spectra for each sample.**

197

198 Interestingly, the activity *vs.* temperature correlation (Figure 4A) serves as a calibration
199 curve for the indirect evaluation of local gradients occurring under irradiation conditions (Figure
200 2B). This strategy has been previously used to determine the local heating of magnetic iron oxide
201 nanoparticles under alternating magnetic fields.⁴¹ As presented in Figure 2B, the enzymatic activity
202 of AuNSt@CALB under 3.2 W/cm² laser irradiation was 58% higher than that under non-
203 irradiated conditions at the same bulk temperature (room temperature). We know that the particles

204 under 3.2 W/cm² laser irradiation are only capable to heat the bulk up to 32 °C (Figure 3C).
205 However, a proportional activity enhancement of 58% would correspond to a bulk temperature of
206 roughly 42 °C (see Figure 4A). The differences between the expected activity according to the bulk
207 temperature correlation (Figure 4A) and the measured activity under laser irradiation (Figure 2B)
208 suggest the existence of a local temperature gradient between the AuNSt surface and the bulk. In
209 this way, according to the obtained enzyme activity values, we can estimate a 10 °C gradient
210 difference between the enzyme environment (42 °C) and the bulk (32 °C). This observation may
211 also be related to previous studies describing the inactivation of enzymes immobilized on Au NPs
212 under laser irradiation, likely due to an excess of local heating.^{10,11}

213 Previous studies have described similar observations on the thermal effects promoted by
214 light absorption.¹⁰⁻¹⁵ Recently, the effects of photothermal heating and LSPR excited charge
215 carriers were investigated in plasmonic catalysis,^{4,8,9} but a clear distinction of their contributions
216 remains challenging. This is because photothermal heating is largely unavoidable following LSPR
217 excitation.⁴² In the present case, AuNSt seem to release more photothermal heating to the
218 surrounding media as a result of a more efficient LSPR excitation^{8, 43} leading to a larger
219 enhancement in the enzyme activity. Moreover, it is plausible that water pocket interfaces present
220 in the enzyme structure can result in higher yields of energy distribution throughout the enzyme
221 structure.⁴⁴ Lastly, we argue that discussing the activity enhancement mechanism through a
222 mechanism based on LSPR-excited charge carriers would be too speculative, as the hydrolysis
223 mechanism does not involve electron transfer and CALB lacks any metallic center that may
224 facilitate electron shuttle. Although both mechanisms might occur simultaneously, electronic
225 effects can be hardly assessed for this system using state-of-the-art methodologies, whereas
226 photothermal effects are more accessible as we showed.

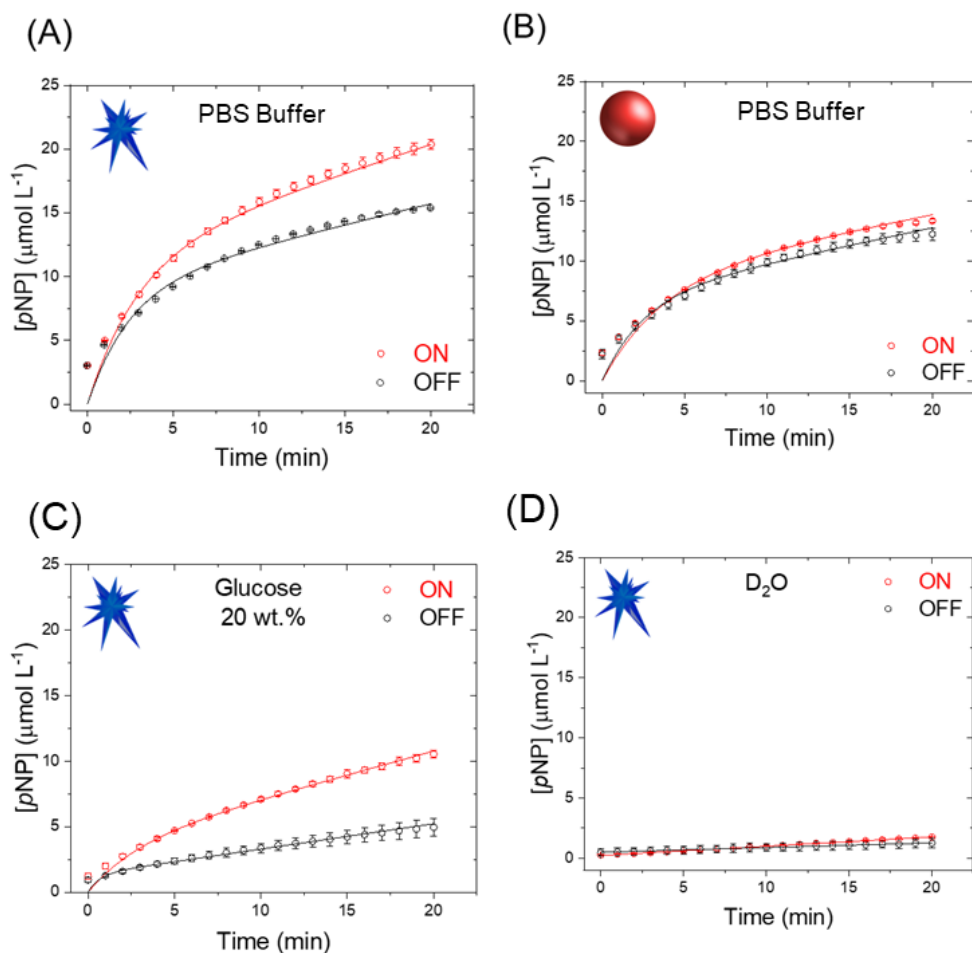
227 Inspired by these results, we performed a series of studies to understand the effect of LSPR
228 excitation on the activity enhancement observed for AuNSt@CALB through determination of the
229 steady-state kinetic parameters under irradiation conditions. First of all, we investigated how the
230 maximum reaction rate and k_{cat} were affected by light irradiation when CALB was adsorbed on
231 Au NPs (Table 1 and Figure S3). The value of the apparent k_{cat} is 60% higher for AuNSt@CALB
232 under irradiation than under non-irradiation conditions. This effect was less noticeable for
233 AuNSp@CALB, and even less for free CALB. Interestingly, K_M values increased under laser
234 irradiation only when CALB was adsorbed on Au NPs, with no apparent changes in free CALB,
235 suggesting that laser irradiation influences the enzymatic activity when CALB is at the Au NPs
236 surface. The k_{cat}/K_M showed similar values for all samples, regardless of light irradiation, because
237 the effect of light on the catalytic constant is compensated by the effect on the binding constant.
238 The higher k_{cat} values under irradiation conditions are probably due to the higher local temperature
239 at the surface of AuNSt, which is also supported by the analysis based on Arrhenius plots (Figure
240 S6). The activation energy barrier for the enzyme activity on AuNSt@CALB decreased from 32
241 to 21 kJ mol⁻¹ when the laser was turned on. In contrast, light was unable to alter the activation
242 energy of the free enzyme, supporting that the interface between the enzyme and AuNSt played a
243 key role to enhance the enzymatic activity through plasmonic effects.

244 We next performed a more detailed analysis of the reaction time-courses that revealed
245 fundamental mechanistic information for the performance of CALB adsorbed on Au NPs, under
246 light irradiation conditions (Figure 5). According to the general enzymatic mechanism (see Figure
247 6), the reaction kinetics are driven by an initial fast equilibrium binding step followed by an
248 irreversible chemical step. Assuming that the second step of the lipase reaction is the rate-limiting
249 one, the activity assay we used does not account for the product release of the acid,^{28,45,46} since the

250 colorimetric method only detects the product *p*NP. The reaction time-courses in Figure 5 were
251 fitted to the initial-burst kinetic model as described by Equation 2, to better estimate the second
252 step of the lipase mechanism.⁴⁷

$$253 \quad [P] = vt + [E_0] * (1 - e^{-k_{obs}t}) \quad (2)$$

254 Here, the concentration of the formed product (P) is related to the initial velocity (*v*), the initial
255 concentration of the enzyme (*E*₀), and the rate constant (*k*_{obs}), as a function of time (*t*) (see Figure
256 S7). In this kinetic model, if *k*_{obs} >> *v*, *v* accounts for the rate-limiting step in the enzymatic
257 mechanism of CALB, which we assign to the steps of hydrolysis of the acyl-enzyme complex and
258 product release. Looking beyond the initial burst in the early stages of product conversion with
259 AuNSt@CALB, Figure 5A illustrates that light irradiation affects more significantly the second
260 phase (after ca. 5 min) of the time-courses. Indeed, AuNSt@CALB exhibited a *v* value which is
261 36% higher under irradiation than under non-irradiation (dark) conditions. Such a light-driven
262 enhancement was higher than that observed for AuNSp@CALB (12%). The time-course
263 conversion as a function of time for free CALB did not fit this kinetic model, but the Michaelis-
264 Menten kinetic parameters clearly demonstrate that the activity of the free enzyme was not affected
265 by light irradiation. Consequently, laser irradiation appears to play a relevant role in the rate-
266 limiting step of the enzyme reaction mechanism.



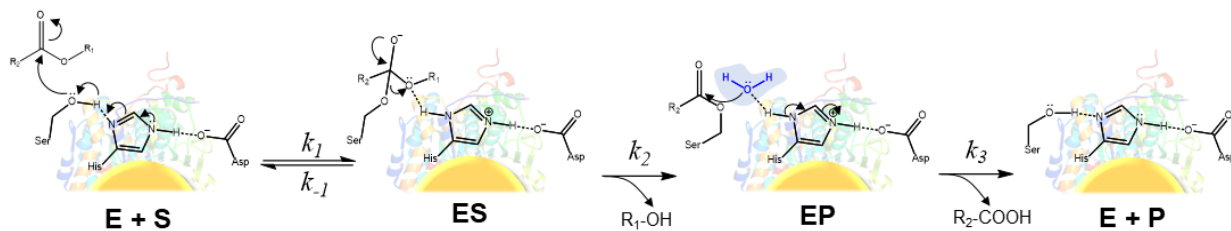
267

268 **Figure 5.** Time-courses of pNPP hydrolysis catalyzed in PBS buffer (A and B) by AuNSt@CALB
 269 (A, C and D) and AuNSp@CALB (B), under NIR irradiation (3.2 W/cm^2) and non-irradiation
 270 (dark) conditions. Viscosity (C) and solvent isotopic (D) effects on the time dependence of the
 271 product formation for AuNSt@CALB. Viscosity assays were performed in presence of glucose 20
 272 wt.% and solvent isotopic assays were performed in the presence of D_2O . All experimental data
 273 were fitted to an initial-burst kinetic model (Equation 2) and the respective values are listed in
 274 Table S1.

275

276 To explain the effect of light on CALB activity from a mechanistic point of view, we
 277 inspected the well-known three-step catalytic mechanism of hydrolases (Figure 6).^{23, 26, 45, 48, 49} This
 278 mechanism is defined by four distinct rate constants (k_1, k_{-1}, k_2, k_3).^{26, 45, 49} Therefore, to decipher
 279 whether light affects either chemical hydrolysis, product release or both steps, reaction time-

280 courses were recorded with AuNSt@CALB in different reaction media, under both light and dark
281 conditions.



283 **Figure 6.** Scheme of the general mechanism for a lipase catalytic reaction. The constants k_1 and k_{-1}
284 are related to reversible binding of the substrate (S) to the enzyme (E) active site, to form the
285 transient intermediate (ES); k_2 rules the formation of the acyl-enzyme complex and release of the
286 alcohol product (EP); k_3 accounts for the hydrolysis of that complex, releasing the acid product to
287 the bulk (E +P).

288

289 We first monitored reaction time-courses in viscous media (20 wt% glucose), aiming at
290 hampering the product diffusion out the active center (state E+P). The interchain hydrogen bonds
291 formed between glucose molecules increase the medium viscosity⁵⁰, like other sugar solutions such
292 as sucrose,^{22, 23} which is known to hamper product release from the enzyme microenvironment.
293 Under these conditions, the product release appears to be the dominant rate-limiting step,^{23, 48} so
294 the effects of laser irradiation on the ν parameter of the initial-burst model compared to the
295 corresponding control experiments (no glucose) can be quantified. Under both on and off
296 conditions, more viscous reaction media slowed down product formation along time (Figure 5C
297 and Table S1). Remarkably, light irradiation significantly accelerated (by 40%) the slowest phase
298 of the time-courses using AuNSt@CALB under viscous conditions. Conversely, the influence of
299 light on the performance of both AuNSp@CALB and free CALB was negligible (Figure S8). To
300 confirm the results extracted from the burst-kinetic model, and considering the deacylation of the
301 enzyme as the slower step (*i.e.*, $k_3 \ll k_2$), which means that k_3 is the rate-limiting step (*i.e.*, $k_{\text{cat}} =$

302 k_3) as supported by recent computational studies⁵¹, we constructed the three-step kinetic model
303 showed in Figure 6 using the software COPASI.⁵² This model allowed us to estimate k_3 values
304 from the reaction courses obtained with AuNSt@CALB (see Table S2 and Figure S9). We found
305 that k_3 follows the same trend as the ν parameter calculated from the initial-burst kinetic model.
306 Light increases by 2-fold the k_3 value of AuNSt@CALB, compared to the non-irradiated reaction,
307 and the $k_{3(\text{ON})}/k_{3(\text{OFF})}$ ratio is maximized under viscous reaction media (in the presence of glucose)
308 by a factor of 3.5 (Figure S10). These experimental results suggest that light contributes to
309 enhancing the catalytic properties of AuNSt@CALB through easing the product release (state
310 E+P) from enzyme close to the plasmonic NPs surface. Subsequently, to evaluate whether light
311 can also affect the kinetics of the hydrolytic step (state EP), the kinetic isotopic effect (KIE)⁵³ was
312 studied by using heavy water (D_2O) under laser on and off conditions, and the results were
313 compared to their corresponding control experiments (in H_2O). In this step, water molecules from
314 the medium play a crucial role in the nucleophilic attack for cleaving the carbonyl group bond of
315 the acyl-enzyme complex.^{26, 49} When using D_2O as solvent, the enzyme activity dramatically
316 decreased for both conditions, as expected from the occurrence of an isotopic effect in the
317 hydrolysis step⁵³ (Figure 5D). Hence, we observe a KIE of $\nu(\text{H}_2\text{O})/\nu(\text{D}_2\text{O})$ of 8.67, which
318 demonstrates that the hydrolysis of the acyl-enzyme complex dominates the rate-limiting step (k_3).
319 On the other hand, when the reaction time-courses were recorded in the presence of D_2O and under
320 irradiation conditions, light had a negligible effect on the enzymatic rates. Hence, when the
321 hydrolysis of the acyl-enzyme complex is extremely slow due to isotopic effects, NIR laser
322 irradiation no longer affects the rate-limiting step of the AuNSt@CALB catalysis mechanism.
323 Interestingly, these results indicate that plasmonic excitation hardly affects the kinetics of water
324 attack, while it significantly increases the efficiency of the product release step. When compared

325 to the activity of soluble CALB measured in PBS buffer, we found a stronger temperature
326 dependence of the free enzyme activity in viscous media, but a weaker dependence in D₂O. These
327 results further support the enhancement of product release when the enzyme is locally heated at the
328 interface with the irradiated plasmonic nanoparticle (Figure S11). Previous studies reporting that
329 enzyme immobilization on the surface of nanoparticles leads to more significant changes in the
330 product release step in the enzymatic kinetics^{22, 23} also support the assumption that the major
331 contribution of light is related to this step. Therefore, our results demonstrate that LSPR excitation
332 increases the activity of AuNSt@CALB by enhancing the kinetics of product release in the last
333 step of the enzyme mechanism driven by k_3 , as summarized in Figure 6. This effect has been
334 observed exclusively with AuNSt@CALB, confirming that the LSPR of Au NPs must be in
335 resonance with the incident NIR laser wavelength (808 nm), to exert the effect on enzyme
336 properties.

337 CONCLUSION

338 We used CALB adsorbed on the surface of Au nanospheres (NSp) and nanostars (NSt) as
339 a model system to unravel the effect of light illumination, and thus LSPR excitation, on the
340 underlying mechanisms behind the plasmonic enhancement of enzyme activity under NIR
341 excitation. It was found that LSPR excitation in the NIR enabled an increase of 58% in enzyme
342 activity when Au NSt were employed as immobilization carriers. In addition to the enhanced
343 activities, we investigated the effect of plasmonic excitation on the rate-limiting step of the
344 enzymatic reaction. Data from highly viscous conditions and solvent isotopic effects revealed that
345 photothermal heating from LSPR excitation accelerated the latest step of the reaction by favoring
346 product release, rather than improving the hydrolytic step at the interface between the enzyme and
347 the plasmonic NPs. We envision that some of the mechanistic conclusion reached in this work can

348 be translated to other combinations of enzymes and plasmonic NPs, and may inspire the rational
349 design of plasmonic NPs and enzyme hybrids with target activities and selectivity that can be
350 externally controlled by light excitation.

351 EXPERIMENTAL SECTION

352 **Materials.** Lipase from *Candida antarctica* fraction B (CALB), tetrachloroauric acid
353 ($\text{HAuCl}_4 \cdot 3\text{H}_2\text{O}$), sodium citrate tribasic dihydrate, ascorbic acid, silver nitrate, 4-nitrophenyl
354 palmitate were purchased from Sigma-Aldrich. Phosphate-buffered saline was purchased from
355 Biochrom GmbH, (Berlin, Germany). CALB solutions were prepared in PBS buffer pH 7.4. The
356 concentration of CALB was determined by the colorimetric kit Bradford assay⁵⁴, purchased from
357 Thermo Scientific. All chemicals were used as received. Purified Milli-Q water (Millipore, 18.2
358 $\text{M}\Omega \text{ cm}$) was used in the preparation of all solutions.

359 **Gold nanoparticles synthesis and CALB adsorption.**

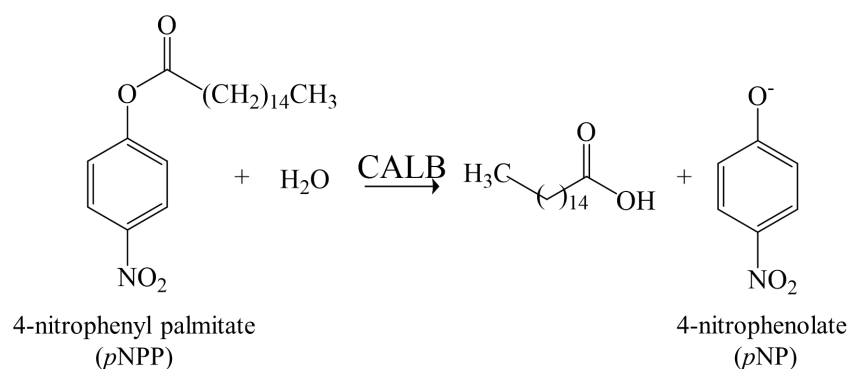
360 *AuNSp@CALB synthesis.* AuNSp were obtained by Turkevich method.⁵⁵ In a typical procedure,
361 150 mL of 2.2 mmol L^{-1} sodium citrate solution under vigorous stirring was heated until boiling.
362 Then, 1 mL of 25 mmol L^{-1} $\text{HAuCl}_4 \cdot 3\text{H}_2\text{O}$ was added. The temperature was decreased to $\sim 90^\circ\text{C}$
363 and the solution color change from soft yellow to red in ~ 10 min. After the solution reach 90°C ,
364 1 mL of 60 mmol L^{-1} sodium citrate solution and 1 mL of 25 mmol L^{-1} $\text{HAuCl}_4 \cdot 3\text{H}_2\text{O}$ were
365 subsequently added, and let it stir during 30 min at 90°C . After cooling to room temperature,
366 samples were stored in fridge for further use. The adsorption of CALB onto AuNSp to obtain
367 AuNSp@CALB bioconjugates was adapted from a previously described method.²⁴ First, 0.1 mg
368 mL^{-1} CALB stock solutions were prepared in PBS buffer pH 7.4. 10 mL of CALB solution was
369 added to 10 mL of previously synthesized AuNSp. The sample was incubated during 2h at 32°C

370 and 300 rpm in an Eppendorf thermomixer. After, before using, the colloidal dispersion was
371 washed by centrifugation at 13 000 rpm during 20 min to remove the excess of CALB and possible
372 non-reactants from AuNSp synthesis. The precipitate was washed and re-dispersed in PBS buffer.
373 Samples were previous analyzed by UV-Vis spectroscopy (Agilent 8453) to monitor the LSPR
374 signal and to determine the molar gold concentration in the samples at $\lambda = 400 \text{ nm}^{38}$.
375 AuNSp@CALB final concentration of Au was $0.84 \mu\text{mol L}^{-1}$ and of CALB was $1.06 \mu\text{mol L}^{-1}$.

376 *AuNSt@CALB synthesis.* AuNSt@CALB synthesis were adapted from a previously described
377 method.^{33,34} AuNSt were obtained by seed-mediated growth. Firstly, seed solution was prepared
378 by adding 5 mL of 34 mmol L^{-1} sodium citrate into 95 mL of 0.5 mmol L^{-1} $\text{HAuCl}_4 \cdot 3\text{H}_2\text{O}$ under
379 boiling and vigorous stirring, and it was let stirring during 15 min at the same temperature and
380 stirring. After cooling to room temperature, the colloidal dispersion was stored in fridge for further
381 use. For AuNSt synthesis, 100 μL of 25 mmol L^{-1} $\text{HAuCl}_4 \cdot 3\text{H}_2\text{O}$ was added into 10 mL of H_2O
382 containing 10 μL of 1 mmol L^{-1} HCl under vigorous stirring at room temperature. Then, 100 μL
383 of seed solution, 100 μL of 3 mmol L^{-1} silver nitrate solution and 50 μL of 100 mmol L^{-1} ascorbic
384 acid solution were quickly subsequent added. After 3-5 min of stirring, 10 mL of 0.1 mg mL^{-1}
385 CALB solution was added and let it stirring for 5 min. Then, the sample was stored in fridge for
386 further use. Samples were washed just before the use by centrifugation at 7000 rpm during 15 min
387 to remove the excess of CALB and possible non-reactants from AuNSt synthesis. The precipitate
388 was washed and re-dispersed in PBS buffer. Samples were previous analyzed by UV-Vis
389 spectroscopy (Agilent 8453) to monitor the LSPR signal and to determine the molar gold
390 concentration in the samples at $\lambda = 400 \text{ nm}^{38}$. AuNSt@CALB final concentration of Au was 0.54
391 $\mu\text{mol L}^{-1}$ and of CALB was $1.14 \mu\text{mol L}^{-1}$.

392 **Enzymatic activity assays.**

393 *pNPP hydrolysis time dependence of the product formation.* Enzymatic activity of free CALB and
394 CALB-AuNSp bioconjugates were determined by measuring the release of 4-nitrophenolate (*p*NP)
395 from the hydrolysis of 4-nitrophenyl palmitate (*p*NPP) (Scheme 1), monitored by UV-Vis
396 spectroscopy at $\lambda = 405$ nm, as previously described elsewhere.^{24,26} In a quartz cuvette containing
397 1000 μ L of PBS buffer pH 7.4, 36 μ L of 0.5 mmol L⁻¹ *p*NPP solution previously prepared in
398 isopropanol was added. All *p*NPP solutions were prepared in the same day before use.
399 Subsequently, 36 μ L of the sample was added and homogenized. The solution change slowly from
400 transparent to light yellow upon *p*NP release, according to the amount of CALB in the sample.
401 *p*NP concentration was determined from Lambert-Beer's law using molar extinction coefficient of
402 $\epsilon = 12800$ mol L⁻¹ cm⁻¹.²⁶ The enzymatic activity was determined from the initial velocity obtained
403 from the linear slope of *p*NP concentration versus time plot. The unit U/g corresponds to 1 μ mol
404 of the product *p*NP formed per 1 min of reaction related to the amount of protein. For the assays
405 upon laser illumination, the cuvette was illuminated vertically (see illustrative scheme in Figure
406 2A) and measures of the absorbance of *p*NP formation were recorded at each 1 min during
407 approximately 20 min.



Scheme 1. Hydrolysis of pNPP biocatalyzed by CALB. The reaction rate can be monitored from pNP formation, by monitoring absorbance at $\lambda = 405$ nm.

408

409 *Michaelis-Menten.* Enzymatic kinetics of free CALB and CALB-AuNPs bioconjugates were
 410 determined by the typical procedure of Michaelis-Menten model^{28, 56}. First, pNPP solutions at
 411 initial concentrations of 0.5, 0.4, 0.3, 0.2, 0.1, 0.05, and 0.01 mmol L⁻¹ were prepared in
 412 isopropanol. All pNPP solutions were prepared at the same day before use. The same procedure
 413 described in the previous topic for pNPP hydrolysis time dependence of the product formation to
 414 determine the enzyme activity was performed. The values of the parameters maximum velocity
 415 (V_{\max}) and Michaelis-Menten constant (K_M), related to the initial velocity (V_o) and substrate
 416 concentration ($[S]$), were obtained from the typical relation:

417
$$V_o = \frac{V_{\max} * [S]}{K_M + [S]} \quad (3)$$

418 *Arrhenius.* Arrhenius analysis was performed to determine the enzyme activation energy of free
 419 CALB and CALB-AuNPs bioconjugates as described previously elsewhere²². The enzyme activity
 420 was determined by the same procedure described in the former topic for pNPP hydrolysis, varying
 421 the temperature from 25 to 80 °C. The values of activation energy (E_a) were obtained from the
 422 linear fitting from the relation described as

423
$$\ln K = \ln A - \frac{E_a}{RT} \quad (4)$$

424 where, k is the rate constant, A is the pre-exponential factor, R is the universal gas constant at the
425 absolute temperature (T).

426 *Viscosity and solvent isotope dependence.* Viscosity and solvent isotope dependence kinetics were
427 performed as previous described elsewhere.^{23,48} For the viscosity assays, kinetics was performed
428 in presence of 20 wt% glucose prepared in PBS buffer. For the solvent isotope assays, kinetics was
429 performed in presence of D₂O and all samples were previously washed and re-suspended in D₂O
430 to avoid any water molecules at the kinetics. Enzyme activity was determined by the same
431 procedure described in the previous topic for pNPP hydrolysis time dependence of the product
432 formation. Data were analyzed and fitted by an initial-burst of product kinetics model.⁴⁷

433 **Heating experiments.** 1 mL of sample in a quartz cuvette was illuminated by a near-infrared laser
434 at $\lambda = 808$ nm (fiber-coupled laser diode, Lumics LU0808T040) laterally, passing through two
435 lenses, one to collimate and other to expand the laser beam in order to illuminate a spot of 1 cm²
436 onto the sample. The laser was illuminated upon different powers (0.7, 1.6, and 3.2 W/cm²) and
437 monitored by using a thermal camera (FLIR A35) above the cuvette. The heating and cooling
438 curves were obtained from the thermal camera data by using the ResearchIR software. PBS buffer
439 and water were measured as blank curves to eliminate any contribution from the medium. The
440 molar heat rate transfer was calculated by the relation³⁷:

441
$$\frac{\Delta Q}{c_{Au}} = \frac{Q_{sample} - Q_{medium}}{\epsilon_{400}/2.4 \text{ mmolL}^{-1}} \quad (5)$$

442 where, the generated heat output (ΔQ), obtained from the difference of heat from the sample
443 (Q_{sample}) and from the medium (Q_{medium}), is related in terms of the estimate gold concentration (c_{Au}
444 $= \epsilon_{400}/2.4 \text{ mmol L}^{-1}$)³⁸ in the sample.

445 **Characterization techniques.**

446 *Transmission electron microscopy (TEM)*. TEM images were obtained by using a JEOL
447 microscope at an acceleration voltage of 200 kV. Approximately 3 μL of sample was dropped on
448 a lacey carbon-coated grid and left to dry. The size distribution of nanoparticles obtained were
449 analyzed by using ImageJ software.

450 *Circular dichroism (CD) spectroscopy*. CD measurements were obtained in a Jasco J-815 CD
451 spectrometer. CD spectra were recorded in the range 200-260 nm, using a quartz cuvette of 5 mm,
452 bandwidth of 5 nm, data pitch of 1 nm, scanning speed at 50 nm/min. The spectra were obtained
453 by an average of 10 accumulations and corrected by the PBS buffer spectrum. The measurements
454 were showed in molar residue ellipticity (MRE) by using the relation:

$$455 \quad MRE = \frac{MRW \times \theta}{10dC} \quad (6)$$

456 where, the measured ellipticity (θ) in degrees is related to the cuvette path length (d) in centimeters
457 and the protein concentration (C) in g mL^{-1} . MRW corresponds to the mean residue weight defined
458 by $MRW = M / (N-1)$, where M is the molecular mass in Daltons and N is the number of amino
459 acids in the protein structure. For CALB, $M = 33000 \text{ g mol}^{-1}$ and $N = 317$.⁴⁰

460

461 ASSOCIATED CONTENT

462 **Supporting Information.**

463 The following files are available free of charge.

464 Additional information of LSPR characterization before and after NIR laser irradiation; Michaelis-
465 Menten plots; NIR laser power effect on free CALB; CD spectra as function of temperature;
466 Arrhenius plots, example of initial-burst of product kinetics; viscosity on time dependence of the
467 product formation; fitting data carried out with COPASI and the values obtained; Table containing
468 parameters obtained from kinetics fitted data and from COPASI software (PDF)

469 **AUTHOR INFORMATION**

470 **Corresponding Author**

471 Heloise R. Barros - Department of Fundamental Chemistry, Institute of Chemistry, University of
472 São Paulo, Av. Prof. Lineu Prestes, 748, Vila Universitária, 05508-000 São Paulo, SP, Brazil; CIC
473 biomaGUNE, Basque Research and Technology Alliance (BRTA), Paseo de Miramón 182, 20014
474 Donostia – San Sebastián, Spain. Email: barroshr@usp.br

475 Fernando López-Gallego - CIC biomaGUNE. Basque Research and Technology Alliance (BRTA),
476 Paseo de Miramón 182, 20014 Donostia – San Sebastián, Spain; Ikerbasque, Basque Foundation
477 for Science, 48013 Bilbao, Spain. Email: flopez@cicbiomagune.es

478 **Author Contributions**

479 The manuscript was written through contributions of all authors. All authors have given approval
480 to the final version of the manuscript.

481 **Notes**

482 The authors declare no competing financial interest.

483 ACKNOWLEDGMENT

484 Authors thank Brazilian agencies CNPq and São Paulo Research Foundation FAPESP
485 (2015/26308-7, 2018/13492-2) for financial support. HRB also thanks FAPESP for the fellowships
486 granted (2019/09668-0, 2017/20892-4). PHCC thanks FAPESP, the University of Helsinki, and
487 the Jane and Aatos Erkko Foundation for support. CK thanks funding from the European Union's
488 Horizon 2020 research and innovation program under the Marie Skłodowska-Curie grant
489 agreement No. 799393 (NANOBIOME). LML-M and IG acknowledges funding from the Spanish
490 State Research Agency (Grant MAT2017-86659-R). Funding from IKERBASQUE to LML-M
491 and FLG is also acknowledged. This work was performed under the Maria de Maeztu Units of
492 Excellence Program from the Spanish State Research Agency – Grant No. MDM-2017-0720.

493 ABBREVIATIONS

494 Au NPs, gold nanoparticles; AuNSp, gold nanospheres; AuNSt, gold nanostars; CALB, *Candida*
495 *antarctica* fraction B; CD, circular dichroism; k, rate constant; k_{cat} , apparent catalytic rate; k_{cat}/K_M ,
496 catalytic efficiency; KIE, kinetic isotopic effect; K_M , Michaelis constant; LSPR, localized surface
497 plasmon resonance; MRE, mean residue ellipticity; NIR, near-infrared; *p*NP, 4-nitrophenolate;
498 *p*NPP, 4-nitrophenyl palmitate; TEM, transmission electron microscopy.

499

500 REFERENCES

501 1. Mosquera, J.; Zhao, Y.; Jang, H. J.; Xie, N. L.; Xu, C. L.; Kotov, N. A.; Liz-Marzán,
502 L. M., Plasmonic Nanoparticles with Supramolecular Recognition. *Advanced Functional*
503 *Materials* **2020**, *30* (2).

- 504 2. Litti, L.; Reguera, J.; de Abajo, F. J. G.; Meneghetti, M.; Liz-Marzan, L. M.,
505 Manipulating chemistry through nanoparticle morphology. *Nanoscale Horizons* **2020**, *5* (1), 102-
506 108.
- 507 3. Bodelon, G.; Costas, C.; Perez-Juste, J.; Pastoriza-Santos, I.; Liz-Marzan, L. M., Gold
508 nanoparticles for regulation of cell function and behavior. *Nano Today* **2017**, *13*, 40-60.
- 509 4. Liz-Marzan, L. M.; Murphy, C. J.; Wang, J. F., Nanoplasmonics. *Chemical Society*
510 *Reviews* **2014**, *43* (11), 3820-3822.
- 511 5. Araujo, T. P.; Quiroz, J.; Barbosa, E. C. M.; Camargo, P. H. C., Understanding
512 plasmonic catalysis with controlled nanomaterials based on catalytic and plasmonic
513 metals *Current Opinion in Colloid & Interface Science* **2019**, *39*, 110-122.
- 514 6. Linic, S.; Aslam, U.; Boerigter, C.; Morabito, M., Photochemical transformations on
515 plasmonic metal nanoparticles. *Nature Materials* **2015**, *14* (6), 567-576.
- 516 7. Wang, H.; Liu, T.; Huang, Y. Z.; Fang, Y. R.; Liu, R. C.; Wang, S. X.; Wen, W. J.;
517 Sun, M. T., Plasmon-driven surface catalysis in hybridized plasmonic gap modes. *Scientific*
518 *Reports* **2014**, *4*.
- 519 8. Baffou, G.; Quidant, R., Thermo-plasmonics: using metallic nanostructures as nano-
520 sources of heat. *Laser & Photonics Reviews* **2013**, *7* (2), 171-187.
- 521 9. Baffou, G.; Quidant, R., Nanoplasmonics for chemistry. *Chemical Society Reviews* **2014**,
522 *43* (11), 3898-3907.
- 523 10. Guo, S. J.; Li, H.; Liu, J.; Yang, Y. M.; Kong, W. Q.; Qiao, S.; Huang, H.; Liu, Y.;
524 Kang, Z. H., Visible-Light-Induced Effects of Au Nanoparticle on Laccase Catalytic Activity.
525 *Acs Applied Materials & Interfaces* **2015**, *7* (37), 20937-20944.
- 526 11. Bretschneider, J. C.; Reismann, M.; von Plessen, G.; Simon, U., Photothermal Control
527 of the Activity of HRP-Functionalized Gold Nanoparticles. *Small* **2009**, *5* (22), 2549-2553.
- 528 12. Blankschien, M. D.; Pretzer, L. A.; Huschka, R.; Halas, N. J.; Gonzalez, R.; Wong, M.
529 S., Light-Triggered Biocatalysis Using Thermophilic Enzyme-Gold Nanoparticle Complexes.
530 *Acs Nano* **2013**, *7* (1), 654-663.
- 531 13. Li, W.; Liu, D. N.; Geng, X.; Li, Z. Q.; Gao, R. J., Real-time regulation of catalysis by
532 remote-controlled enzyme-conjugated gold nanorod composites for aldol reaction-based
533 applications. *Catalysis Science & Technology* **2019**, *9* (9), 2221-2230.
- 534 14. Tadepalli, S.; Yim, J.; Madireddi, K.; Luang, J. Y.; Naik, R. R.; Singamaneni, S., Gold
535 Nanorod-Mediated Photothermal Enhancement of the Biocatalytic Activity of a Polymer-
536 Encapsulated Enzyme. *Chemistry of Materials* **2017**, *29* (15), 6308-6314.
- 537 15. Tadepalli, S.; Yim, J.; Cao, S. S.; Wang, Z. Y.; Naik, R. R.; Singamaneni, S., Metal-
538 Organic Framework Encapsulation for the Preservation and Photothermal Enhancement of
539 Enzyme Activity. *Small* **2018**, *14* (7).
- 540 16. Yang, S. Y.; Yao, D. F.; Wang, Y. S.; Yang, W. T.; Zhang, B. B.; Wang, D. B.,
541 Enzyme-triggered self-assembly of gold nanoparticles for enhanced retention effects and
542 photothermal therapy of prostate cancer. *Chemical Communications* **2018**, *54* (70), 9841-9844.
- 543 17. Khiavi, M. A.; Safary, A.; Aghanejad, A.; Barar, J.; Rasta, S. H.; Golchin, A.; Omidi,
544 Y.; Somi, M. H., Enzyme-conjugated gold nanoparticles for combined enzyme and photothermal
545 therapy of colon cancer cells. *Colloids and Surfaces a-Physicochemical and Engineering Aspects*
546 **2019**, *572*, 333-344.
- 547 18. Yang, K. K.; Liu, Y. J.; Wang, Y.; Ren, Q. L.; Guo, H. Y.; Matson, J. B.; Chen, X.
548 Y.; Nie, Z. H., Enzyme-induced in vivo assembly of gold nanoparticles for imaging-guided
549 synergistic chemo-photothermal therapy of tumor. *Biomaterials* **2019**, *223*.

- 550 19. Barros, H. R.; López-Gallego, F.; Liz-Marzán, L. M., Light-Driven Catalytic Regulation
551 of Enzymes at the Interface with Plasmonic Nanomaterials. *Biochemistry Article ASAP* **2020**.
- 552 20. Nel, A. E.; Madler, L.; Velegol, D.; Xia, T.; Hoek, E. M. V.; Somasundaran, P.;
553 Klaessig, F.; Castranova, V.; Thompson, M., Understanding biophysicochemical interactions at
554 the nano-bio interface. *Nature Materials* **2009**, *8* (7), 543-557.
- 555 21. Ansari, S. A.; Husain, Q., Potential applications of enzymes immobilized on/in nano
556 materials: A review. *Biotechnology Advances* **2012**, *30* (3), 512-523.
- 557 22. Breger, J. C.; Ancona, M. G.; Walper, S. A.; Oh, E.; Susumu, K.; Stewart, M. H.;
558 Deschamps, J. R.; Medintz, I. L., Understanding How Nanoparticle Attachment Enhances
559 Phosphotriesterase Kinetic Efficiency. *Acs Nano* **2015**, *9* (8), 8491-8503.
- 560 23. Breger, J. C.; Oh, E.; Susumu, K.; Klein, W. P.; Walper, S. A.; Ancona, M. G.;
561 Medintz, I. L., Nanoparticle Size Influences Localized Enzymatic Enhancement-A Case Study
562 with Phosphotriesterase. *Bioconjugate Chemistry* **2019**, *30* (7), 2060-2074.
- 563 24. de Barros, H. R.; Santos, M. C.; Barbosa, L. R. S.; Piovan, L.; Riegel-Vidotti, I. C.,
564 Physicochemical Study of the Interaction between Gold Nanoparticles and Lipase from *Candida*
565 sp. (CALB): Insights into the Nano-Bio Interface. *Journal of the Brazilian Chemical Society*
566 **2019**, *30* (10), 2231-2242.
- 567 25. Kisukuri, C. M.; Palmeira, D. J.; Rodrigues, T. S.; Camargo, P. H. C.; Andrade, L. H.,
568 Bimetallic Nanoshells as Platforms for Metallo- and Biometallo-Catalytic Applications.
569 *Chemcatchem* **2016**, *8* (1), 171-179.
- 570 26. Wu, C. S.; Wu, C. T.; Yang, Y. S.; Ko, F. H., An enzymatic kinetics investigation into
571 the significantly enhanced activity of functionalized gold nanoparticles. *Chemical*
572 *Communications* **2008**, (42), 5327-5329.
- 573 27. Baumann, V.; Muhammed, M. A. H.; Blanch, A. J.; Dey, P.; Rodriguez-Fernandez, J.,
574 Biomolecules in Metal and Semiconductor Nanoparticle Growth. *Israel Journal of Chemistry*
575 **2016**, *56* (4), 195-213.
- 576 28. Johnson, B. J.; Algar, W. R.; Malanoski, A. P.; Ancona, M. G.; Medintz, I. L.,
577 Understanding enzymatic acceleration at nanoparticle interfaces: Approaches and challenges.
578 *Nano Today* **2014**, *9* (1), 102-131.
- 579 29. Song, Y. H.; Chen, J. Y.; Liu, H. Y.; Song, Y. G.; Xu, F. G.; Tan, H. L.; Wang, L.,
580 Conformation, Bioactivity and Electrochemical Performance of Glucose Oxidase Immobilized
581 on Surface of Gold Nanoparticles. *Electrochimica Acta* **2015**, *158*, 56-63.
- 582 30. Lopez-Tobar, E.; Hernandez, B.; Ghomi, M.; Sanchez-Cortes, S., Stability of the
583 Disulfide Bond in Cystine Adsorbed on Silver and Gold Nanoparticles As Evidenced by SERS
584 Data. *Journal of Physical Chemistry C* **2013**, *117* (3), 1531-1537.
- 585 31. Hakkinen, H., The gold-sulfur interface at the nanoscale. *Nature Chemistry* **2012**, *4* (6),
586 443-455.
- 587 32. Irani, M.; Tornvall, U.; Genheden, S.; Larsen, M. W.; Hatti-Kaul, R.; Ryde, U., Amino
588 Acid Oxidation of *Candida antarctica* Lipase B Studied by Molecular Dynamics Simulations and
589 Site-Directed Mutagenesis. *Biochemistry* **2013**, *52* (7), 1280-1289.
- 590 33. de Aberasturi, D. J.; Serrano-Montes, A. B.; Langer, J.; Henriksen-Lacey, M.; Parak,
591 W. J.; Liz-Marzán, L. M., Surface Enhanced Raman Scattering Encoded Gold Nanostars for
592 Multiplexed Cell Discrimination. *Chemistry of Materials* **2016**, *28* (18), 6779-6790.
- 593 34. Yuan, H. K.; Khoury, C. G.; Hwang, H.; Wilson, C. M.; Grant, G. A.; Vo-Dinh, T.,
594 Gold nanostars: surfactant-free synthesis, 3D modelling, and two-photon photoluminescence
595 imaging. *Nanotechnology* **2012**, *23* (7).

- 596 35. Turkevich, J.; Stevenson, P. C.; Hillier, J., A STUDY OF THE NUCLEATION AND
597 GROWTH PROCESSES IN THE SYNTHESIS OF COLLOIDAL GOLD. *Discussions of the*
598 *Faraday Society* **1951**, (11), 55-&.
- 599 36. Kheirloom, A.; Khorasheh, F.; Fazelinia, H., Influence of external mass transfer
600 limitation on apparent kinetic parameters of penicillin G acylase immobilized on nonporous
601 ultrafine silica particles. *Journal of Bioscience and Bioengineering* **2002**, *93* (2), 125-129.
- 602 37. Kuttner, C.; Holler, R. P. M.; Quintanilla, M.; Schnepf, M. J.; Dulle, M.; Fery, A.;
603 Liz-Marzan, L. M., SERS and plasmonic heating efficiency from anisotropic core/satellite
604 superstructures. *Nanoscale* **2019**, *11* (38), 17655-17663.
- 605 38. Hendel, T.; Wuithschick, M.; Kettemann, F.; Birnbaum, A.; Rademann, K.; Polte, J.,
606 In Situ Determination of Colloidal Gold Concentrations with UV-Vis Spectroscopy: Limitations
607 and Perspectives. *Analytical Chemistry* **2014**, *86* (22), 11115-11124.
- 608 39. Daniel, R. M.; Danson, M. J., Temperature and the catalytic activity of enzymes: A fresh
609 understanding. *Febs Letters* **2013**, *587* (17), 2738-2743.
- 610 40. Rabbani, G.; Ahmad, E.; Khan, M. V.; Ashraf, M. T.; Bhat, R.; Khan, R. H., Impact of
611 structural stability of cold adapted *Candida antarctica* lipase B (CaLB): in relation to pH,
612 chemical and thermal denaturation. *Rsc Advances* **2015**, *5* (26), 20115-20131.
- 613 41. Armenia, I.; Bonavia, M. V. G.; De Matteis, L.; Ivanchenko, P.; Martra, G.; Gornati,
614 R.; de la Fuente, J. M.; Bernardini, G., Enzyme activation by alternating magnetic field:
615 Importance of the bioconjugation methodology. *Journal of Colloid and Interface Science* **2019**,
616 *537*, 615-628.
- 617 42. Jain, P. K., Taking the Heat Off of Plasmonic Chemistry. *Journal of Physical Chemistry*
618 *C* **2019**, *123* (40), 24347-24351.
- 619 43. Chatterjee, H.; Rahman, D. S.; Sengupta, M.; Ghosh, S. K., Gold Nanostars in
620 Plasmonic Photothermal Therapy: The Role of Tip Heads in the Thermoplasmonic Landscape.
621 *Journal of Physical Chemistry C* **2018**, *122* (24), 13082-13094.
- 622 44. Leitner, D. M.; Pandey, H. D.; Reid, K. M., Energy Transport across Interfaces in
623 Biomolecular Systems. *Journal of Physical Chemistry B* **2019**, *123* (45), 9507-9524.
- 624 45. Johnson, K. A., A century of enzyme kinetic analysis, 1913 to 2013. *Febs Letters* **2013**,
625 *587* (17), 2753-2766.
- 626 46. Powers, K. T.; Washington, M. T., Analyzing the Catalytic Activities and Interactions of
627 Eukaryotic Translesion Synthesis Polymerases. *DNA Repair Enzymes: Structure, Biophysics,*
628 *and Mechanism* **2017**, *592*, 329-356.
- 629 47. Hammes, G.; Hammes-Schiffer, S., *Physical chemistry for the biological sciences*. 2nd
630 edition ed.; John Wiley & Sons.; New Jersey, 2015; Vol. 55.
- 631 48. Gadda, G.; Fitzpatrick, P. F., Solvent isotope and viscosity effects on the steady-state
632 kinetics of the flavoprotein nitroalkane oxidase. *Febs Letters* **2013**, *587* (17), 2785-2789.
- 633 49. Jaeger, K. E.; Dijkstra, B. W.; Reetz, M. T., Bacterial biocatalysts: Molecular biology,
634 three-dimensional structures, and biotechnological applications of lipases. *Annual Review of*
635 *Microbiology* **1999**, *53*, 315-+.
- 636 50. Telis, V. R. N.; Telis-Romero, J.; Mazzotti, H. B.; Gabas, A. L., Viscosity of aqueous
637 carbohydrate solutions at different temperatures and concentrations. *International Journal of*
638 *Food Properties* **2007**, *10* (1), 185-195.
- 639 51. Galmes, M. A.; Garcia-Junceda, E.; Swiderek, K.; Moliner, V., Exploring the Origin of
640 Amidase Substrate Promiscuity in CALB by a Computational Approach. *Acs Catalysis* **2020**, *10*
641 (3), 1938-1946.

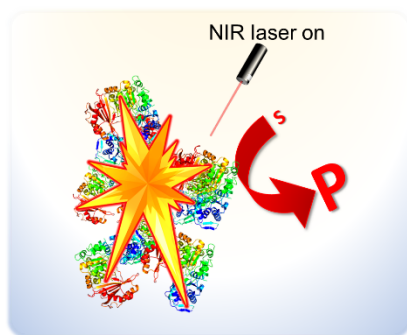
- 642 52. Hoops, S.; Sahle, S.; Gauges, R.; Lee, C.; Pahle, J.; Simus, N.; Singhal, M.; Xu, L.;
643 Mendes, P.; Kummer, U., COPASI- A COMplex PATHway SIMulator. *Bioinformatics* **2006**, *22*
644 (24), 3067-3074.
- 645 53. Quinn, D. M., SOLVENT ISOTOPE EFFECTS FOR LIPOPROTEIN-LIPASE
646 CATALYZED-HYDROLYSIS OF WATER-SOLUBLE PARA-NITROPHENYL ESTERS.
647 *Biochemistry* **1985**, *24* (13), 3144-3149.
- 648 54. Bradford, M. M., RAPID AND SENSITIVE METHOD FOR QUANTITATION OF
649 MICROGRAM QUANTITIES OF PROTEIN UTILIZING PRINCIPLE OF PROTEIN-DYE
650 BINDING. *Analytical Biochemistry* **1976**, *72* (1-2), 248-254.
- 651 55. Bastus, N. G.; Comenge, J.; Puntès, V., Kinetically Controlled Seeded Growth Synthesis
652 of Citrate-Stabilized Gold Nanoparticles of up to 200 nm: Size Focusing versus Ostwald
653 Ripening. *Langmuir* **2011**, *27* (17), 11098-11105.
- 654 56. Johnson, K. A.; Goody, R. S., The Original Michaelis Constant: Translation of the 1913
655 Michaelis-Menten Paper. *Biochemistry* **2011**, *50* (39), 8264-8269.

656

657

658

659 FOR TABLE OF CONTENTS ONLY



660

661 **Plasmonic biocatalysis:** control of enzyme activity by LSPR excitation of plasmonic
662 nanoparticles using external light irradiation.

663